Bifurcation Instability in Linear Elasticity with the Constraint of Local Injectivity*

Roger Fosdick[1], Francesco Freddi[2], Gianni Royer-Carfagni[2]

[1] Department of Aerospace Engineering and Mechanics
University of Minnesota
Minneapolis, MN 55455
USA

[2] Department of Civil-Environmental Engineering
and Architecture
University of Parma
Parco Area delle Scienze 181/A, I
43100 Parma
Italia

Abstract. There are problems in linear elasticity theory whose corresponding deformations, usually associated with singular stress fields, are open to question because they are not one-to-one and predict self-intersection. Recently, a theory has been advanced to handle such situations, which consists in minimizing the quadratic energy functional of linear elasticity subject to the constraint of local injectivity. In particular, the Jacobian of the deformation gradient is required to be not less than an arbitrarily small positive quantity, and, thus, the local orientation is preserved. Here, this theory is applied to the classical Lekhnitskii problem of an elastic aelotropic circular disk which is loaded on its boundary by a uniform radial pressure. Without the injectivity constraint, this classical linear problem has a unique solution. This example, with the injectivity constraint, already has been considered in previous works, but radial symmetry was assumed in order to reduce the problem from 2D to 1D. Here, making use of an interior penalty formulation, a numerical scheme is implemented that solves a full 2D problem. Remarkably, it is shown that there are values of the material moduli for which the minimal potential energy solution is no longer symmetric, producing a strong azimuthal shear and nominally a 180° rotation of an internal central core of the disk. Although the elastic strain energy is quadratic and convex, the strongly nonlinear character of the constraint allows for bifurcation instabilities.

*We gratefully acknowledge the partial support of the *Minnesota Supercomputing Institute* and the Italian "Ministero per l'Università e la Ricerca Scientifica" under the program PRIN 2005 "Affidabilità di elementi in vetro strutturale: indagini teoriche e sperimentali sulla risposta termo-meccanica del materiale e di strutture trasparenti di tipo innovativo". R.F. gratefully acknowledges the Department of Civil and Environmental Engineering at the *Politecnico di Bari*, Italy, for their kind hospitality and support during his visit of 2006.

Key Words Linear elasticity, anisotropic plate, constraint minimization, penalty method, FEM, bifurcation instability

MSC 2000 classification 75B05, 74E10, 74G65, 74G70, 74S05

1 Introduction.

Many classical solutions from linear elasticity theory that are associated with singular stress fields are commonly and widely employed in engineering applications. The stress singularities produce singularities in the corresponding strain field, so that the major assumption for the linear theory that the displacement gradient is infinitesimal is violated. However, even a more insidious consequence is that there are cases for which the corresponding deformation field is not one-to-one no matter how small are the prescribed tractions and/or displacements at the boundary, thus producing a seemingly paradoxical rejection of one of the main pillars of continuum mechanics. Such spurious behavior has been underlined in [2] for the situation of plane strain in the case of a bonded rigid punch which is pushed into a isotropic linear elastic half space. The anomalous response was therein partially solved by resorting to two special non-linear elasticity theories.

An alternative approach was advanced in [7], where it was proposed to minimize the classical quadratic potential energy functional of linear elasticity subject to the constraint of local injectivity. This requires that the determinant of the deformation gradient is not less than an arbitrary small positive quantity ε, and implies that the orientation of the deformation is locally preserved. As a paradigmatic example of the relevant theory, the authors presented a classical problem, already discussed by Lekhnitskii [8], i.e., the problem of an aelotropic circular disk in plane strain or generalized plane stress, radially compressed along its external contour by a uniformly distributed normal force p per unit length. For a cylindrically aelotropic material, which has one axis of orthotropic material symmetry coinciding with the radial direction, it can be shown easily that the elastic solution may become singular at the disk center. The elasticity tensor is not continuous at the disk center because for such a material symmetry it has a different constant value on each radial line of the disk. It can thus be shown that there are values of the elastic moduli for which material overlapping may occur.

This problem represents an interesting example of an irregular solution of an elliptic system of partial differential equations with bounded coefficients, of the kind evidenced by De Giorgi in a famous counterexample [5]. De Giorgi's work invalidated some overly optimistic conjectures on the regularity of weak solutions of elliptic systems, conjectures based upon the known result that a solution in the 1D case is a Hlder-continuous function if the coefficients of the differential equation are bounded [10]. De Giorgi [5] showed that such a result cannot be extended to the multi-dimensional case by inventing a counterexample wherein he exhibited an unbounded and discontinuous extremal for a variational system of elliptic equations with discontinuous, though bounded, coefficients. Later, De Giorgi's counterexample was interpreted in the framework of linear elastostatics by Podio-Guidugli [13]. In Lekhnitskii's problem the elastic coefficients are bounded, but discontinuous at the center of the disk where there is a conflicting convergence of material symmetries. The corresponding displacement field is continuous but the strain, and consequently the stress, grows unboundedly at the disk center. Thus, there are regions where self-intersection and material overlapping may occur.

In order to overcome the difficulty of material overlapping, recently, in [15], it was proposed to consider a compound circular disk with a homogenous isotropic linear elastic inner core. No stress singularity occurs at the center in this case because the elastic moduli, i.e., the coefficients of the corresponding elliptic system of equations, are continuous at the center. Nevertheless, the author of [15] neglected to notice that material overlapping indeed occurs for an inner isotropic core of non-zero radius (this point will be discussed in detail in Section 2). Moreover, contrary to what is stated in [15], as the radius of the inner core tends to zero the corresponding sequence of elastic solutions approaches Lekhnitskii's singular, self-intersecting solution and no advantage is gained with this approach.

The Lekhnitskii problem, with the local orientation preserving constraint of local injectivity, was solved in closed form in [7] using the assumption of radial symmetry: when the displacement is radially symmetric, the problem can be reduced to an ordinary differential equation. In this solution, the constraint is active in a central core of the disk, forcing the deformation field to respect the injectivity requirement. Moreover, the corresponding Lagrange multiplier field was found to act as a Cauchy isotropic stress (pressure) in the central core, remindful of the fact that the force between the atoms of a material becomes strongly repelling when the separation distance between them is made sufficiently small.

The analytical solution of the constrained Lekhnitskii problem was confirmed by the numerical solution of [6] wherein a Lagrange multiplier technique was used. However, considerable difficulties were encountered in this work because of the strongly nonlinear character of the constraint, which involves the determinant of the deformation gradient. A Newton-Raphson method was used to iteratively solve the resulting system of equations, and it was very likely that the initial approximate at each step of the iterative procedure violated the injectivity constraint. On the other hand, the constraint acted as a "barrier" in that it required any successive approximate to return to the set of admissible deformations. In other words, when an approach toward the solution was attempted from the exterior of the domain of the constraint, serious numerical instabilities were stimulated. This problem was by-passed by forcing "by hand" the numerical approximations to stay in the domain of the constraint. However, this procedure would be difficult to apply if the actual solution is not known in advance and the domain in the body in which the constraint is active is completely unknown.

An alternative, more efficient numerical approach was considered in [1] by using a so-called *interior penalty formulation*. This approach requires one to determine a displacement field which minimizes an augmented potential energy functional, i.e., the potential energy of linear elasticity plus a penalty functional [14] divided by a sufficiently large penalty parameter. A sequence of minimizers, parameterized by the penalty parameter, is then constructed which converges to the solution of the constrained minimization problem when the parameter tends to infinity. This approach, at least in theory, has the advantage that the Newton-Raphson method can be implemented at each step to minimize the penalized functional, without having to control that each approximate remains in the class of locally injective functions. However, in practice, one has to control that, at each iteration, the step length is chosen small enough to remain inside the admissible set. In any case, this control does not introduce additional numerical difficulties. Using again the assumption of radial symmetry, and thus reducing the problem to one of one-dimension, the constrained minimization problem was solved in [1], arriving at complete agreement with the analytical analysis of [7].

In this paper the numerical solution of the constrained Lekhnitskii problem is again considered using the interior penalty formulation of [1], but the main novelty is that now

the full two-dimensional problem is considered, without applying the assumption of radial symmetry. The well-known radially symmetric solution is in some cases recovered but, remarkably, it is shown that there are values for the elastic moduli for which the corresponding minimizing deformation is no longer radially symmetric. This is due to the fact that, although the elastic strain energy is quadratic and convex, the strongly nonlinear character of the constraint allows for the occurrence of bifurcation instabilities. Radially symmetric and non-symmetric solutions are discussed in detail. Difficulties in the numerical solution of the full 2D problem, which were not considered in [1], are revealed.

2 The Lekhnitskii disk problem

2.1 The Lekhnitskii's solution

A paradigmatic example in two dimensions where the injectivity requirement is violated has been recorded by Lekhniskii [8]. This work considered the equilibrium of a cylindrically aelotropic linear elastic disk of radius R_0 with fixed center point which is radially compressed along its external contour by a uniformly distributed normal force p per unit length. A singularity of stress at the center point was recorded for certain elastic moduli, but self-intersection in the neighborhood of the center was not noticed. In the following, we shall use cylindrical coordinates (with origin at the fixed disk center). The notation is shown in Figure 1: A point $\mathbf{X} = (R, \Theta)$ in the reference configuration at which the orthonormal cylindrical basis is $(\mathbf{e}_r(\mathbf{X}), \mathbf{e}_\theta(\mathbf{X}))$ is mapped to the point $\mathbf{x} = (r, \theta)$ at which the orthonormal basis is $(\mathbf{e}_r(\mathbf{x}), \mathbf{e}_\theta(\mathbf{x}))$.

In linear theory, the stress

$$\mathbf{T} = \sigma_{rr}\mathbf{e}_r(\mathbf{X}) \otimes \mathbf{e}_r(\mathbf{X}) + \sigma_{r\theta}(\mathbf{e}_r(\mathbf{X}) \otimes \mathbf{e}_\theta(\mathbf{X}) + \mathbf{e}_\theta(\mathbf{X}) \otimes \mathbf{e}_r(\mathbf{X})) + \sigma_{\theta\theta}\mathbf{e}_\theta(\mathbf{X}) \otimes \mathbf{e}_\theta(\mathbf{X}) \,,$$

and the strain

$$\mathbf{E} = e_{rr}\mathbf{e}_r(\mathbf{X}) \otimes \mathbf{e}_r(\mathbf{X}) + e_{r\theta}(\mathbf{e}_r(\mathbf{X}) \otimes \mathbf{e}_\theta(\mathbf{X}) + \mathbf{e}_\theta(\mathbf{X}) \otimes \mathbf{e}_r(\mathbf{X})) + e_{\theta\theta}\mathbf{e}_\theta(\mathbf{X}) \otimes \mathbf{e}_\theta(\mathbf{X}) \,,$$

are related by

$$\begin{aligned} \sigma_{rr} &= c_{11}e_{rr} + c_{12}e_{\theta\theta} \,, \\ \sigma_{\theta\theta} &= c_{21}e_{rr} + c_{22}e_{\theta\theta} \,, \\ \sigma_{r\theta} &= 2c_{66}e_{r\theta} \,, \end{aligned} \tag{2.1}$$

where the elastic moduli c_{11},c_{22}, $c_{12} = c_{21}$ and c_{66} are constant. By simple inversion, one obtains

$$\begin{aligned} e_{rr} &= \frac{1}{E_r}\sigma_{rr} - \frac{\nu_r}{E_r}\sigma_{\theta\theta} \,, \\ e_{\theta\theta} &= -\frac{\nu_\theta}{E_\theta}\sigma_{rr} + \frac{1}{E_\theta}\sigma_{\theta\theta} \,, \\ e_{r\theta} &= \frac{1}{2G}\sigma_{r\theta} \,, \end{aligned} \tag{2.2}$$

where the technical (engineering) moduli E_r, ν_r, E_θ, ν_θ, and G satisfy

$$c_{11} = \frac{E_r}{1-\nu_r\nu_\theta} \,, \quad c_{22} = \frac{E_\theta}{1-\nu_r\nu_\theta} \,, \quad c_{12} = \frac{E_\theta\nu_r}{1-\nu_r\nu_\theta} \,, \quad c_{21} = \frac{E_r\nu_\theta}{1-\nu_r\nu_\theta} \,, \quad c_{66} = G \,. \tag{2.3}$$

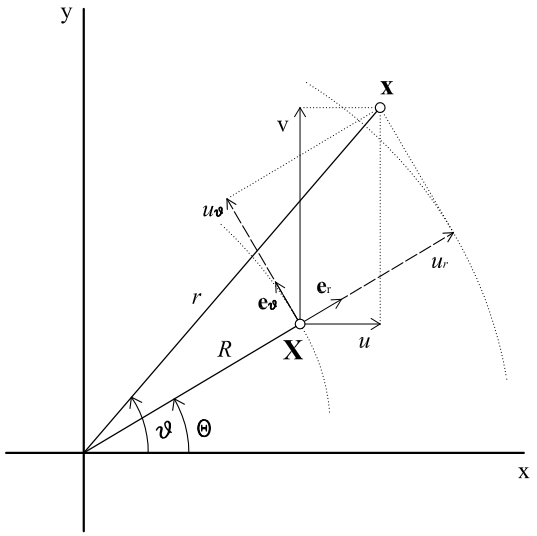

Figure 1: Displacement components according to the orthogonal and cylindrical base vectors.

The symmetry condition $c_{12} = c_{21}$ implies

$$\frac{\nu_r}{E_r} = \frac{\nu_\theta}{E_\theta}\,,$$

and, in order to render the strain energy positive definite, the conditions

$$c_{11} > 0\,, \quad c_{22} > 0\,, \quad c_{66} > 0\,, \quad c_{11}c_{22} - c_{21}c_{12} > 0\,, \tag{2.4a}$$

$$E_r > 0\,, \quad E_\theta > 0\,, \quad G > 0\,, \quad 1 - \nu_r\nu_\theta > 0\,, \tag{2.4b}$$

must hold.

Under these hypotheses, the linear elliptic equations corresponding to the classical equilibrium boundary-value problems of linear elasticity theory have a unique solution, modulo an infinitesimal rotation and translation which depends continuously upon the boundary data. The solution of the Lekhnitskii problem is rotationally symmetric with respect to the center of the disk; the displacement field must be of the form $\mathbf{u} = u(R)\mathbf{e}_r(\mathbf{X})$. Consequently, the strain components are

$$e_{rr} = u_{,R}\,, \quad e_{\theta\theta} = \frac{u}{R}\,, \quad e_{r\theta} = 0\,. \tag{2.5}$$

The one non-trivial equilibrium equation becomes

$$\sigma_{rr,R} + \frac{\sigma_{rr} - \sigma_{\theta\theta}}{R} = 0\,, \tag{2.6}$$

which, because of the constitutive relations (2.1), reduces to the differential equation

$$c_{11}u_{,RR} + \frac{1}{R}c_{11}u_{,R} - c_{22}\frac{u}{R^2} = 0\,. \tag{2.7}$$

By imposing the boundary condition $\sigma_{rr} = -p$ and the condition that the origin is fixed, i.e., $u(0) = 0$, Lekhniskii's solution

$$u(R) = \frac{-p}{(\sqrt{c_{11}c_{22}} + c_{12})R_0^{k-1}} R^k \,, \tag{2.8}$$

is obtained, where the material parameter k is defined as

$$k \equiv \sqrt{\frac{c_{22}}{c_{11}}} = \sqrt{\frac{E_\theta}{E_r}} > 0 \,. \tag{2.9}$$

As a result, when $k < 1$ the radial and hoop stresses are singular for any value of the pressure p because

$$\sigma_{rr} = -p \left(\frac{R}{R_0}\right)^{k-1} \,, \quad \sigma_{\theta\theta} = -pk \left(\frac{R}{R_0}\right)^{k-1} \,. \tag{2.10}$$

An important, and physically unacceptable, response is described by Lekhnitskii's solution when $k < 1$; its importance lies in the fact that it implies material overlapping in a neighborhood of the center of the disk. The deformation of each reference point $\mathbf{X} = (R, \Theta)$ of the disk is given by $\mathbf{x} = \mathbf{f}(\mathbf{X}) = R\mathbf{e}_r(\mathbf{X}) + \mathbf{u}(\mathbf{X})$ and the determinant of the deformation gradient $\nabla\mathbf{f}$ has the form

$$\det\nabla\mathbf{f} = \left[1 - \frac{p}{\sqrt{c_{11}c_{22}} + c_{12}} k \left(\frac{R}{R_0}\right)^{k-1}\right] \left[1 - \frac{p}{\sqrt{c_{11}c_{22}} + c_{12}} \left(\frac{R}{R_0}\right)^{k-1}\right] \,. \tag{2.11}$$

Observe that when $0 < k < 1$ we have $\det\nabla\mathbf{f} < 0$ for

$$\frac{kp}{\sqrt{c_{11}c_{22}} + c_{12}} < \left(\frac{R}{R_0}\right)^{k-1} < \frac{p}{\sqrt{c_{11}c_{22}} + c_{12}} \,. \tag{2.12}$$

Moreover, according to (2.8) there is a core region identified by

$$0 < \left(\frac{R}{R_0}\right)^{k-1} < \frac{p}{\sqrt{c_{11}c_{22}} + c_{12}} \,, \tag{2.13}$$

where $-u(R) > R$. All points belonging to this region are mapped toward and, in fact, through the center of the disk, thus resulting in material interpenetration. Interestingly, although material overlapping occurs in a whole region in the neighborhood of the disk center, the determinant of the deformation gradient is negative only in the annular portion defined in (2.12). The determinant is positive for all points in a central core bounded by this annulus because there is a double overlapping predicted in this region; notice, also, that both the radial and the hoop infinitesimal strains are less that -1 in this region, as readily can be seen from (2.5) and (2.8).

2.2 Lekhnistkii's problem with the constraint of local injectivity

The solution of Lekhnistkii's problem, modified by the constraint of local injectivity, was studied in [7] as an example of a problem of minimum potential energy in linear elasticity theory, where the set of admissible displacement fields is restricted to be locally injective,

i.e., $\det(\mathbf{I}+\nabla\mathbf{u}) \geq \varepsilon > 0$. Relying mainly on Ball's results [3], a general existence theorem for this minimization problem was proved in [7] for the case of two space dimensions.¶

To recall the main results in [7], let $\mathcal{B} \subset \mathbb{R}^2$ denote the undistorted natural configuration of the body under consideration. The boundary $\partial\mathcal{B}$ of $\mathcal{B}$ is partitioned into two non-intersecting parts, $\partial_1\mathcal{B}$ and $\partial_2\mathcal{B}$, $\partial\mathcal{B} \equiv \partial_1\mathcal{B} \cup \partial_2\mathcal{B}$, $\partial_1\mathcal{B} \cap \partial_2\mathcal{B} = \emptyset$, such that $\mathbf{u}(\mathbf{X}) = \bar{\mathbf{u}}(\mathbf{X})$ for $\mathbf{X} \in \partial_1\mathcal{B}$, where $\bar{\mathbf{u}}$ is a given function, and a dead load traction field $\bar{\mathbf{t}}(\mathbf{X})$ is prescribed for $\mathbf{X} \in \partial_2\mathcal{B}$. In addition, a body force $\mathbf{b}(\mathbf{X})$ per unit volume of $\mathcal{B}$ acts at points $\mathbf{X} \in \mathcal{B}$. The minimization problem

$$\min_{\mathbf{u}\in A_\varepsilon} \mathcal{E}[\mathbf{u}] \tag{2.14}$$

is considered, where $\mathcal{E}[\mathbf{u}]$ denotes the classical potential energy functional of linear elasticity theory, i.e.,

$$\mathcal{E}[\mathbf{u}] \equiv \frac{1}{2}\int_{\mathcal{B}} \mathbb{C}[\mathbf{E}]\cdot\mathbf{E}\, dA - \int_{\mathcal{B}} \mathbf{b}\cdot\mathbf{u}\, dA - \int_{\partial\mathcal{B}_2} \bar{\mathbf{t}}\cdot\mathbf{u}\, dS\,, \tag{2.15}$$

and where the class of admissible displacement fields is defined as

$$\mathcal{A}_\varepsilon \equiv \left\{\mathbf{u} \in W^{1,2}(\mathcal{B}) \to \mathbb{R}^2 \,|\, \det(\mathbf{1}+\nabla\mathbf{u}) \geq \varepsilon > 0,\, \mathbf{u} = \bar{\mathbf{u}}(\mathbf{X}) \text{ on } \partial_1\mathcal{B}\right\}. \tag{2.16}$$

Here, $\mathbb{C} = \mathbb{C}(\mathbf{X})$ denotes the positive definite totally symmetric linear transformation of Sym $\to$ Sym, which characterizes the elastic moduli of classical linear elasticity theory, and $\mathbf{E}$ is the infinitesimal strain tensor field

$$\mathbf{E} \equiv \frac{1}{2}\left(\nabla\mathbf{u} + (\nabla\mathbf{u})^T\right). \tag{2.17}$$

The parameter $\varepsilon > 0$ is to be assigned sufficiently small. If the injectivity constraint in $\mathcal{A}_\varepsilon$ was eliminated, and, consequently, the class of admissible deformations was enlarged, then classical linear elasticity theory would prevail.

Suppose $\mathbf{u}^*(\mathbf{X})$ denotes the displacement field of a solution to the constrained minimization problem defined in (2.14), (2.15) and (2.16), with associated strain field $\mathbf{E}^*(\mathbf{X})$. In general, the minimizing deformation divides $\mathcal{B}$ into two non-intersecting open subregions:

$$\mathcal{B}_> \equiv \text{int}[\{\mathbf{X} \in \mathcal{B} : \det(\mathbf{1} + \det\nabla\mathbf{u}) > \varepsilon\}]\,, \tag{2.18a}$$

$$\mathcal{B}_= \equiv \text{int}[\{\mathbf{X} \in \mathcal{B} : \det(\mathbf{1} + \det\nabla\mathbf{u}) = \varepsilon\}]\,, \tag{2.18b}$$

such that $\mathcal{B} \equiv \mathcal{B}_> \cup \mathcal{B}_= \cup \Sigma$, $\mathcal{B}_> \cap \mathcal{B}_= = \emptyset$, where $\Sigma \equiv \overline{\mathcal{B}}_> \cap \overline{\mathcal{B}}_=$ denotes the dividing interfacial region which separates $\mathcal{B}_>$ and $\mathcal{B}_=$. If we let

$$\mathbf{T}^*(\mathbf{X}) \equiv \mathbb{C}[\mathbf{E}^*(\mathbf{X})]\,, \tag{2.19}$$

denote the relevant stress field, it was shown in [7] that the Euler-Lagrange equations for the constrained minimization problem are of the form

$$\text{Div}\ \mathbf{T}^* + \mathbf{b} = \mathbf{0} \ \text{ in } \mathcal{B}_>\,, \tag{2.20a}$$

$$\text{Div}\ \left(\mathbf{T}^* - \varepsilon\,\lambda^*(\mathbf{1}+\nabla\mathbf{u}^*)^{-T}\right) + \mathbf{b} = \mathbf{0}\,,\ \lambda^* \geq 0 \ \text{ in } \mathcal{B}_=\,, \tag{2.20b}$$

¶The three dimensional case remains unresolved and is particularly troublesome because of the "cubic" nature of the injectivity constraint.

and the natural boundary conditions are

$$\mathbf{T}^*\mathbf{n} + \mathbf{b} = \bar{\mathbf{t}} \ \text{ on } \partial\mathcal{B}_> \cap \partial_2\mathcal{B}\,, \tag{2.21a}$$

$$\left(\mathbf{T}^* - \varepsilon\,\lambda^*(\mathbf{1} + \nabla\mathbf{u}^*)^{-T}\right)\mathbf{n} = \bar{\mathbf{t}} \ \text{ on } \partial\mathcal{B}_= \cap \partial_2\mathcal{B}\,. \tag{2.21b}$$

In addition, the jump condition

$$\left(\mathbf{T}^* - \varepsilon\,\lambda^*(\mathbf{1} + \nabla\mathbf{u}^*)^{-T}\right)_{\Sigma\cap\bar{\mathcal{B}}_=}\mathbf{n} = (\mathbf{T}^*)_{\Sigma\cap\bar{\mathcal{B}}_>}\,\mathbf{n} \tag{2.22}$$

must hold across $\Sigma = \bar{\mathcal{B}}_> \cap \bar{\mathcal{B}}_=$. Here, $\mathbf{n}$ is a unit normal to Σ, and the evaluations $\Sigma \cap \bar{\mathcal{B}}_=$ and $\Sigma \cap \bar{\mathcal{B}}_>$ are to be understood as limits to the dividing interface Σ from within $\mathcal{B}_=$ and $\mathcal{B}_>$, respectively.

The field $\lambda^*(\mathbf{X}) \geq 0$ represents the Lagrange multiplier field associated with the constraint $\det(\mathbf{1} + \nabla\mathbf{u}^*)) \geq \varepsilon > 0$. The fact that the Lagrange multiplier field is non-negative is in agreement with the Kuhn-Tucker conditions consequent to the inequality constraint. In the following, we shall consider this problem numerically.

3 Numerical procedure

The constrained minimization problem just discussed presents some computational difficulties. Apart from the intrinsic nonlinearity associated with the unilateral nature of the constraint, the determinant itself is a strongly nonlinear function of the deformation gradient. Consequently, the minimization problem becomes strongly nonlinear and requires a careful numerical strategy. Referring to the numerical experiments recorded in [1] for the one-dimensional case, we shall employ the same solution technique here, i.e., the interior penalty method. However, since now the simulations will be fully two-dimensional and not restricted to be radially symmetric, a few numerical aspects are analyzed in order to optimize the computational costs and to improve convergence.

3.1 Interior penalty formulation

The basic scheme for the *interior-penalty* (or *barrier*) *method* is the following: We must consider the non-convex optimization problem

$$\min \mathcal{E}[\mathbf{u}], \quad \mathbf{u} \in \mathcal{A}_\varepsilon\,, \tag{3.1}$$

for a convex functional $\mathcal{E}$ on a non-convex manifold $\mathcal{A}_\varepsilon$, and construct an appropriate *barrier* function $F(\mathbf{u})$, defined on the interior of $\mathcal{A}_\varepsilon$ and tending to infinity as $\mathbf{u}$ approaches the boundary of $\mathcal{A}_\varepsilon$, i.e.,

$$F : F[\mathbf{u}] \to \infty \quad \text{for } \mathbf{u} \to \partial\mathcal{A}_\varepsilon\,. \tag{3.2}$$

Based upon this barrier function, the constrained minimization problem (3.1) is then converted to a sequence of unconstrained optimization problems of the form

$$\min \mathcal{E}[\mathbf{u}, \delta], \quad \mathbf{u} \in \mathcal{A}_\varepsilon\,, \tag{3.3a}$$

where

$$\mathcal{E}\,[\mathbf{u}, \delta] \equiv \mathcal{E}\,[\mathbf{u}] + \frac{1}{\delta}F\,[\mathbf{u}]\,, \tag{3.3b}$$

and where $\delta > 0$ is the barrier parameter, which is to be sequenced through larger and larger values.

If $\mathbf{u}^*(\delta)$ denotes a minimizer of $\mathcal{E}[\mathbf{u}, \delta]$ then, under appropriate conditions, it can be shown that as $\delta \to \infty$ any limit point $\mathbf{u}^*$ of the sequence $\{\mathbf{u}^*(\delta)\}$ is a solution of (3.1). Moreover, the penalty formulation furnishes an approximation of the Lagrange multiplier field associated with the original constrained problem (3.1). The quality of the approximation improves as the parameter δ is made larger.

As an interior penalty functional appropriate for controlling the constraint of local injectivity, we take the functional

$$F[\mathbf{u}] \equiv \int_{\mathcal{B}} \frac{1}{\det(\mathbf{1} + \nabla\mathbf{u}) - \varepsilon}\, dA \qquad \forall\, \mathbf{u} \in \mathcal{A}_\varepsilon\,. \tag{3.4}$$

As noted in [1], the main advantage of the proposed strategy consists in the fact that each of the approximating sequence of problems defined in (3.3) can be solved using well known algorithms in unconstrained nonlinear theory.

Referring to [1] for the detailed optimization discussion, here we simply recall that a possible approximation λ_δ of the Lagrange multiplier field λ^* defined in (2.20), (2.21) and (2.22) is

$$\lambda_\delta = \frac{1}{\delta\,(\det\nabla(\mathbf{1} + \nabla\mathbf{u}) - \varepsilon)^2}\,. \tag{3.5}$$

It can be verified [1] that $\lambda_\delta \to 0$ in $\mathcal{B}_>$ and, clearly we have $\lambda_\delta \geq 0$ in $\mathcal{B}_=$ as $\delta \to \infty$. This is in agreement with the necessary condition in the second of (2.20).

3.2 Finite Element approximation

For numerical implementation, the minimization of (3.3) is replaced by the search for a solution of a finite number of algebraic nonlinear equations with a finite number of unknowns. In the finite element method framework, these equations are a result of replacing the function space where the problem is set by a finite dimensional approximating subspace, i.e., a subspace $\mathcal{V}_h$ spanned by a set of basis functions $\{\psi_i\}$ defined on a grid work whose size is characterized by h. The discrete version of the penalized potential given by (3.1) and (3.3) may be written in the form

$$\mathcal{E}_h[\mathbf{u}, \delta] = \mathcal{E}_h[\mathbf{u}] + \frac{1}{\delta} F_h[\mathbf{u}]\,, \tag{3.6}$$

where the significance of $\mathcal{E}_h[\mathbf{u}]$ and $F_h[\mathbf{u}]$ is that integrals (2.15) and (3.4) are evaluated by considering the approximation of the displacement field $\mathbf{u}$ in $\mathcal{V}_h$ and, consequently, depend upon the adopted discretization of the domain. Using a standard procedure, minimizers of $\mathcal{E}_h[\mathbf{u}, \delta]$ in $\mathcal{V}_h$ are then characterized by using the weak form of the Euler-Lagrange equations for $\mathcal{E}_h[\mathbf{u}, \delta]$, i.e., test functions are considered in $\mathcal{V}_h$, so that the problem is finally reduced to a nonlinear system of algebraic equations.

In the present work, we shall use a well-known Q_2 approximation, i.e., the elemental displacement field $\mathbf{u}$, as well as the geometry, is approximated by a polynomial of order two and a quadrilateral mesh is adopted. Recall that, as a triangulation is refined, a Q_p mapping approximates the boundary to within an order h^{p+1}, where p is the order of the polynomial and h is the mesh width. The constrained Lehknitski problem has a circular external boundary and in this case the convergence is quite accurate, being of the order of h^{p+2}.[‖] In particular, as shown in Figure 2, as a first choice of mesh size the external

[‖] This order is easily demonstrated by expanding in series the analytical expression of a circle. The cubic term in this expression vanishes, so that the truncation error, which should be cubic for a quadratic mapping ($p = 2$), is instead of the fourth order. Consequently, the convergence order is raised to 4, instead of 3.

boundary is divided into 128 segments (Figure 2a), and a very fine mesh is adopted at the central core of the disk (Figure 2b), where the characteristic size h of the smallest element is of the order of 10^{-7}. However, as we will show later in Section 4.2, there is a special range of choices of the elastic moduli for which the numerical solution becomes particularly difficult and requires a much finer mesh. The importance of the choice of the mesh for problems of this kind has been clearly outlined in [1] and [6].

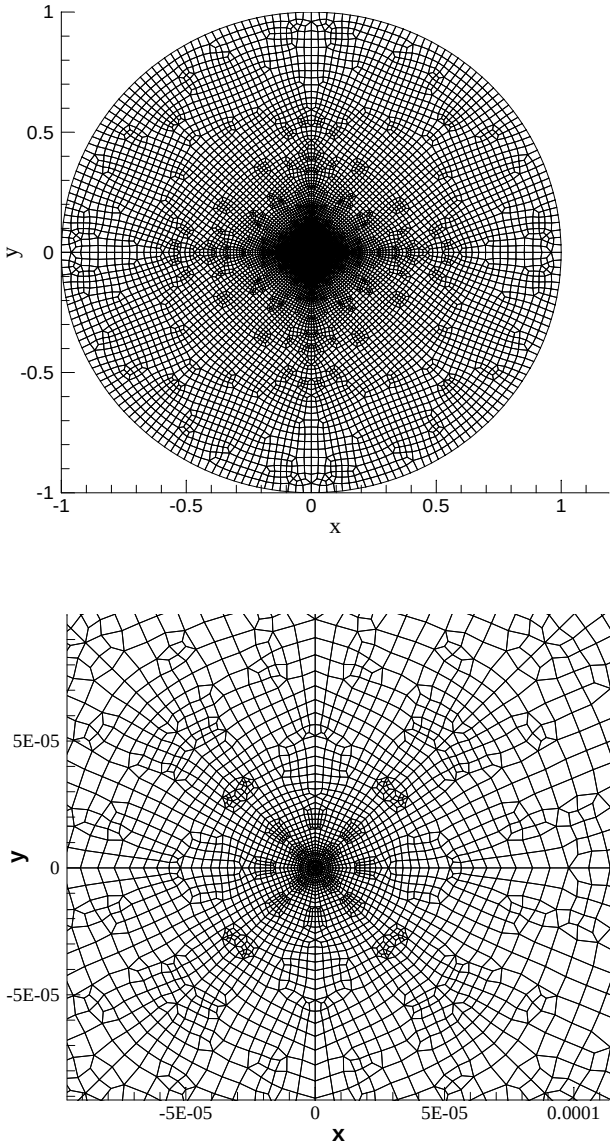

Figure 2: A first choice of FEM mesh used to model the disk: a. The complete mesh; b. A magnification at the disk center.

3.3 Nonlinear solution scheme

The discrete minimization problem is solved iteratively by using a well-known procedure adopted in the (unconstrained) optimization method of [9], here briefly summarized.

Starting from an initial choice of displacement field $\mathbf{u}_0$ that respects the injectivity constraint, a sequence of approximations is generated. At each iteration step $k \geq 0$, the method requires the computation of a *search direction* $\mathbf{p}_k$ and then it decides how far to perturb $\mathbf{u}_k$ in that direction. The iteration is given by

$$\mathbf{u}_{k+1} = \mathbf{u}_k + \alpha_k \mathbf{p}_k \,, \tag{3.7}$$

where the positive scalar $\alpha_k \in \mathbb{R}$ is called the step length. The success of a *line search method* depends upon an effective choice of both the direction $\mathbf{p}_k$, which need not be a unit vector, and the step length α_k. In general, $\alpha = \alpha_k$ corresponds to the scalar that minimizes (3.6) in the affine set $\mathbf{u}_k + \alpha \mathbf{p}_k$ for all $\alpha \in \mathbb{R}$.

Most of the line search algorithms require that $\mathbf{p}_k$ be a "descendent" direction, i.e., one for which

$$D\mathcal{E}_h[\mathbf{u}_k, \delta] \cdot \mathbf{p}_k = \frac{d}{d\lambda} \mathcal{E}_h[\mathbf{u}_k + \lambda \mathbf{p}_k, \delta]_{|\lambda=0} < 0 \,.$$

Of course, this property guarantees that the function $\mathcal{E}_h[\mathbf{u}, \delta]$ becomes smaller by advancing away from $\mathbf{u} = \mathbf{u}_k$ in this direction. In particular, the search direction can be chosen as

$$\mathbf{p}_k = -\mathbf{B}_k^{-1} D\mathcal{E}_h[\mathbf{u}_k, \delta] \,, \tag{3.8}$$

where $\mathbf{B}_k$ is a symmetric and nonsingular matrix. In the steepest descend method $\mathbf{B}_k$ is simply the identity matrix $\mathbf{I}$, while in Newton's method $\mathbf{B}_k$ is the exact Hessian $DD\mathcal{E}_h[\mathbf{u}_k, \delta]$. In quasi-Newton methods, $\mathbf{B}_k$ is an approximation of the Hessian that is updated at each step by means of a low-rank formula. When $\mathbf{p}_k$ is defined by (3.8) and $\mathbf{B}_k$ is positive definite, one has

$$D\mathcal{E}_h[\mathbf{u}_k, \delta] \cdot \mathbf{p}_k = -\left(\mathbf{B}_k^{-1} D\mathcal{E}_h[\mathbf{u}_k, \delta]\right) \cdot D\mathcal{E}_h[\mathbf{u}_k, \delta] < 0 \tag{3.9}$$

so that $\mathbf{p}_k$ is clearly a descent direction. In our simulations we adopt a standard Newton method.

At each step k, the scalar value α_k is first approximated according to the Wolfe conditions

$$\mathcal{E}_h\left[\mathbf{u}_k + \alpha_k \mathbf{p}_k, \delta\right] \leq \mathcal{E}_h\left[\mathbf{u}_k, \delta\right] + c_1 \alpha_k D\mathcal{E}_h[\mathbf{u}_k, \delta] \cdot \mathbf{p}_k \,, \tag{3.10}$$

$$D\mathcal{E}_h\left[\mathbf{u}_k + \alpha_k \mathbf{p}_k, \delta\right] \cdot \mathbf{p}_k \geq c_2 D\mathcal{E}_h[\mathbf{u}_k, \delta] \cdot \mathbf{p}_k \,, \tag{3.11}$$

where $0 < c_1 < c_2 < 1$. The Wolfe conditions are obtained by coupling the well known Armijo condition (3.10) [12] with a restriction on the slope given by (3.11). It can be proved that there exist step lengths that satisfy the Wolfe conditions for every function $\mathcal{E}_h[\cdot, \delta]$ that is smooth and bounded from below. In the computations of this paper, it suffices to choose the values $c_1 = 10^{-4}$ and $c_2 = 0.9$.

The fulfilment of the local injectivity constraint $\det(\mathbf{I} + \nabla \mathbf{u}) \geq \varepsilon > \mathbf{0}$ is checked at the Gauss points of the discrete domain, i.e., those points used for the numerical integration. In case the constraint is violated, the value of α_k is reduced until injectivity is respected *via* a simple backtracking strategy. This control is very important to check in order to avoid the condition where the iterate $\mathbf{u}_k$ yields a value of the barrier function $F[\mathbf{u}_k]$ that overcomes the barrier defined by (3.2): this event in general produces serious numerical instabilities.

In summary, the numerical approach is carried out in two parts. First, for any fixed δ, the functional $\mathcal{E}_h\left[\mathbf{u}, \delta\right]$ of (3.6) is minimized using the nonlinear optimization procedure

outlined above, until the desired accuracy is obtained. Then, the value of δ is augmented and the corresponding functional $\mathcal{E}_h[\mathbf{u}, \delta]$ is again minimized using the same procedure. The solution of the minimization problem for δ is used as the starting point for the iterative method of the next minimization problem after δ is changed. When the method was first introduced in the 1960's, it was referred to as the *sequential unconstrained minimization technique*. Today the method is better known as the *barrier method* (see [16]).

The solution of the original constrained problem (3.1) is obtained in the limit $\delta \to \infty$. The numerical approximation is said to be "sufficiently accurate" when δ is large enough so that the distance between the solutions of two consecutive minimization problems remains within a prescribed tolerance.

4 Numerical results

In the original Lekhnitskii's problem the disk is radially compressed by a uniform pressure. Here, because it is numerically advantageous, the displacement is assigned on the external boundary. In particular, since the disk is centered at the coordinate origin, we apply the following Dirichlet boundary conditions:

$$\mathbf{u}(\mathbf{X}) = -0.02\mathbf{X} \quad , \quad for \ \ |\mathbf{X}| = R_0 \, . \tag{4.1}$$

We set $\varepsilon = 0.1$ in the local injectivity condition $\det(\mathbf{I} + \nabla\mathbf{u}) \geqslant \varepsilon$ and, for convenience, all lengths are normalized by setting the radius of the disk $R_0 = 1$. The penalty approximation scheme has been implemented in a program based upon the Open Source package deal.II [4]. The mesh we employ is illustrated in Figure 2.

4.1 Symmetric solution

Consider first the elastic parameters listed in Table 1. The numerical simulations confirm that the deformation is radially symmetric and of the type already discussed in [7]. In particular, Figure 3 shows the field $r(R) - R$ corresponding to the exact solution of Lekhnitskii's problem (referred to as the *Lekhnitskii solution*) and to the solution of the constrained problem (referred to as the *symmetric solution*). Figure 3 also shows a third graph (referred to as the *asymmetric solution*) which soon will be discussed. Clearly, Figure 3b shows a magnification of Figure 3a in a neighborhood of the center of the disk. In order to appreciate where Lekhnitskii's solution violates the injectivity condition, the line $r(R) - R = -R$, i.e., $r(R) = 0$, also is plotted: The intersection of the Lehknitskii solution with this line defines the radius of the overlapping region.

c_{11}	c_{12}	c_{22}	c_{66}
$1.e5$	$1.e3$	$1.e4$	$1.e5$

Table 1: Elastic parameters used in the numerical simulation associated with a symmetric solution.

In Figure 4, the determinant of the deformation gradient $J \equiv \det(\mathbf{I} + \nabla\mathbf{u})$ is shown for the *symmetric solution*. Here, it is clear that J becomes negative only in an annular region, although material overlapping occurs in a whole central core. Recall that the determinant is positive in a neighborhood of the center of the disk because, there, the Lehknitskii solution suffers a double intersection and both the radial and the hoop infinitesimal strains are less

than -1. This finding is not completely appreciated in [15], where the main consideration is the issue of stress singularity in an elastic cylinder of cylindrically aelotropic material in plane strain. Noting that the singularity may be attributed to a conflicting definition of anisotropy at $R = 0$, the author then removes this conflict and considers a related problem of a compound cylinder in which the outer cylinder is aeolotropic and the inner core is isotropic. One of the conclusions in [15] is that the displacement field corresponds to a one-to-one deformation mapping in the compound cylinder for all radii of the inner isotropic core. However, such is not the case. In Figure 5, the field $r(R) - R$ is plotted for different isotropic core radii. It is evident that, as the radius of this core goes to zero, the solution tends to the Lekhnitskii solution, which is not regular. Of course, in the isotropic core the radial displacement is a linear function of the distance from the disk center, so that both radial and hoop strains become equal and the determinant of the deformation gradient is positive. However, this positiveness in the core region does not rule out interpenetration for the reasons outlined above.

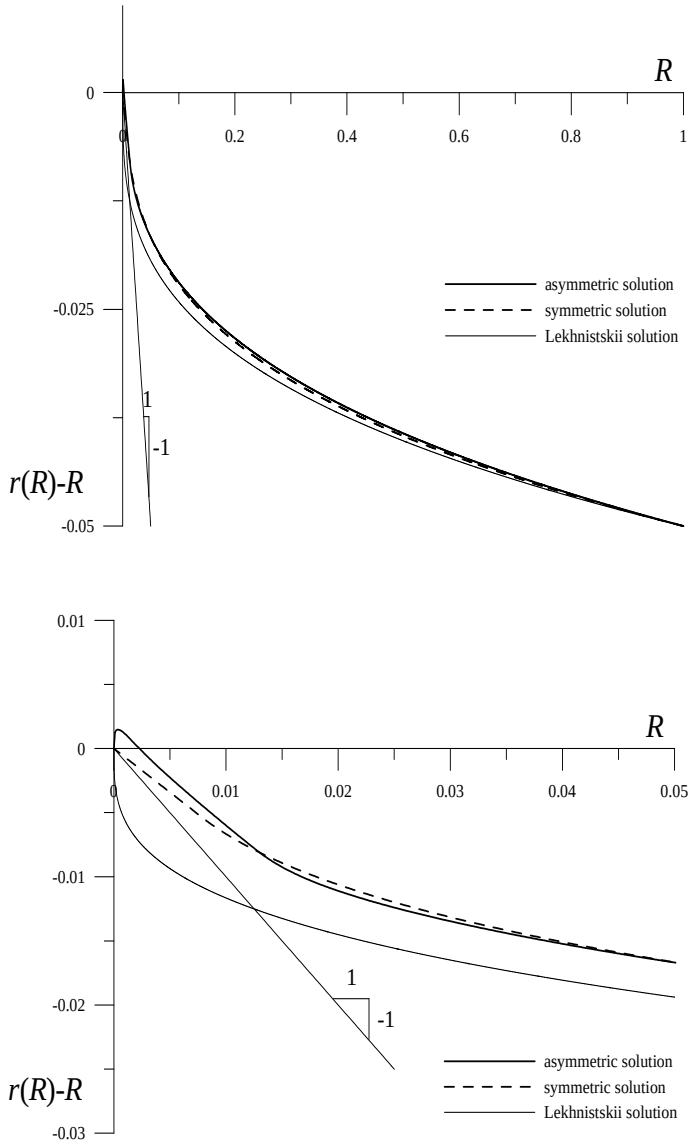

Figure 3: Field $r(R) - R$ for the *Lekhnitskii* solution, for the *symmetric* constrained solution and for the *asymmetric* constrained solution. Two scales of R are shown.

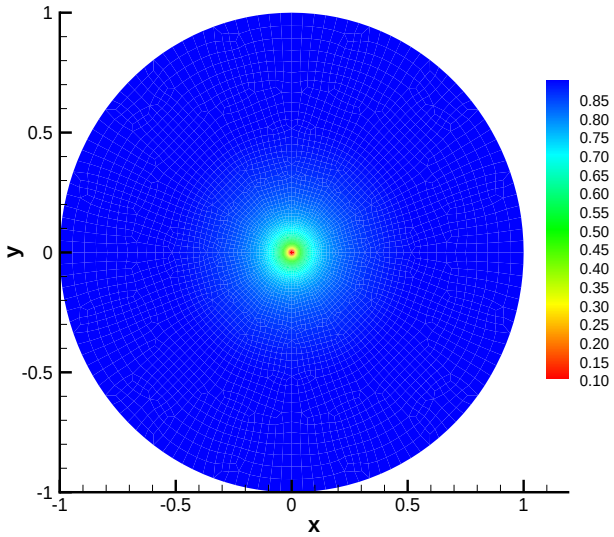

Figure 4: Determinant of the deformation gradient for the symmetric solution.

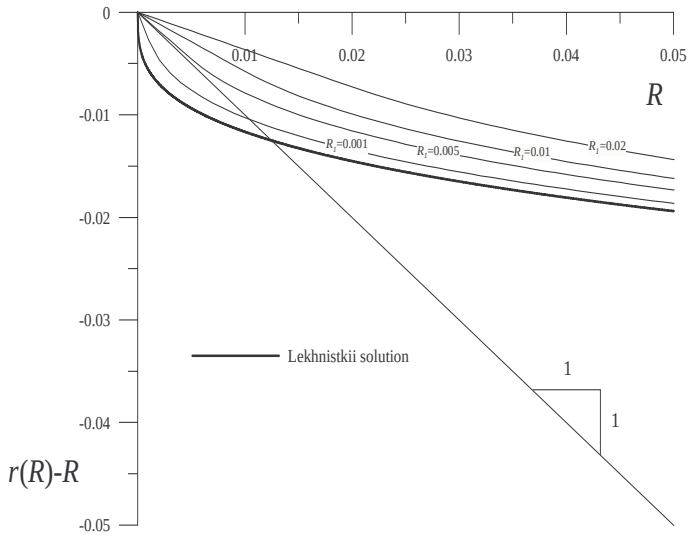

Figure 5: Radial displacement obtained by considering compound disks with inner isotropic cores of different radii R_1, as proposed in [15]. The line $r(R) - R = -R$, i.e., $r(R) = 0$, identifying the overlapping region, is also reported.

4.2 Asymmetric solution

Consider now the case when the elastic parameters are as in Table 2. The difference from Table 1 is that here the shear modulus c_{66} is two orders of magnitude smaller.

c_{11}	c_{12}	c_{22}	c_{66}
$1.e5$	$1.e3$	$1.e4$	$1.e3$

Table 2: Mechanical parameters adopted: Asymmetric solution

Remarkably, the deformation field associated with this case is substantially different from the previous one is that it is no longer radially symmetric. Because of this, such a field will be referred to as the *asymmetric solution*.

The numerical solution now presents considerable difficulties because of the highly nonlinear character of the determinant constraint. Consequently, the disk has been divided into 256 radial sectors and, in particular, we have found it essential to place a super-fine mesh near the center of the disk. The adopted mesh consists of 54912 elements and 55049 nodes. Figure 6 shows a magnification of the deformed mesh in a neighborhood of the origin (recall that the disk radius R_0 has been normalized to 1).

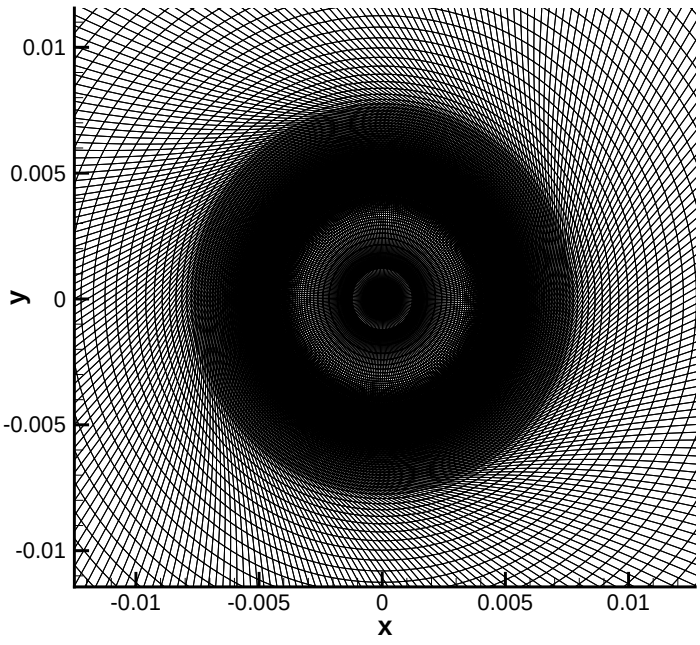

Figure 6: Asymmetric solution: Deformed mesh.

From this figure it is difficult to appreciate the deformation field because the mesh is too refined for the graphic resolution. Figure 7 represents the deformation of a much coarser mesh, indeed the same mesh as shown in Figure 2, which is used here in the asymmetric case only for the convenience of representation; the quantitative numerical results have been generated with the finer mesh of Figure 6. It is evident in Figure 7 that a central core of the disk has rotated in the deformation and, in fact, our computations show that a small central core turns through 180° relative to the external boundary of the disk.

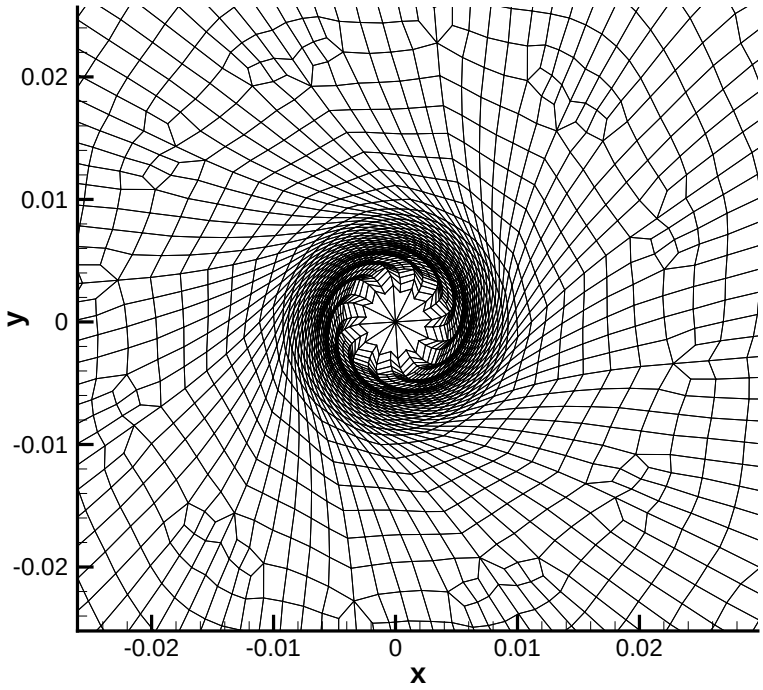

Figure 7: Deformed mesh for the asymmetric solution: Coarse mesh.

In Figure 8, the intensity of the determinant of the deformation gradient $J \equiv \det(\mathbf{I}+\nabla\mathbf{u})$ is shown for the *asymmetric solution*. While only those values of J between 0.1 (the lowest bound) and 0.3 are shown in this figure, our computations show that J takes very large (positive) values in the proximity of the center of the disk and approaches $+\infty$ as $R \to 0$. This singularity of J does not associate with material self-intersection because of the 180° rotation of the core. It is not yet exactly clear what is happening within this core because the mesh converges and, consequently, accuracy of computation is a question. However, it is clear that the material gets onto the other side of the origin not by mapping straight through the origin, as in the Lehknitskii solution, but by rotating 180° aided by a strong region of annular shear in which the injectivity constraint is active. Also, it appears that the deformation gradient is singular. The region where J lies between 0.1 and 0.3 is an annulus and J is greater than 0.3 in the central core as well as outside the annulus. By comparison with Figure 4, we see that the injectivity constraint for the asymmetric solution is active in a region very different from that of the *symmetrical solution*, i.e., the center is no longer constrained.

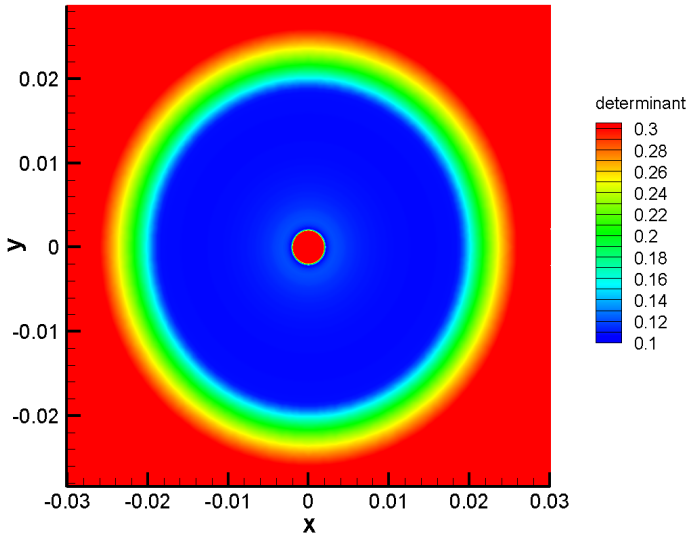

Figure 8: Determinant of the deformation gradient for the asymmetric solution.

The rotation of the central core can be seen in Figures 9a and 9b, which show the displacement component $u_\vartheta(R)$, as defined in Figure 1, for two scales of R.

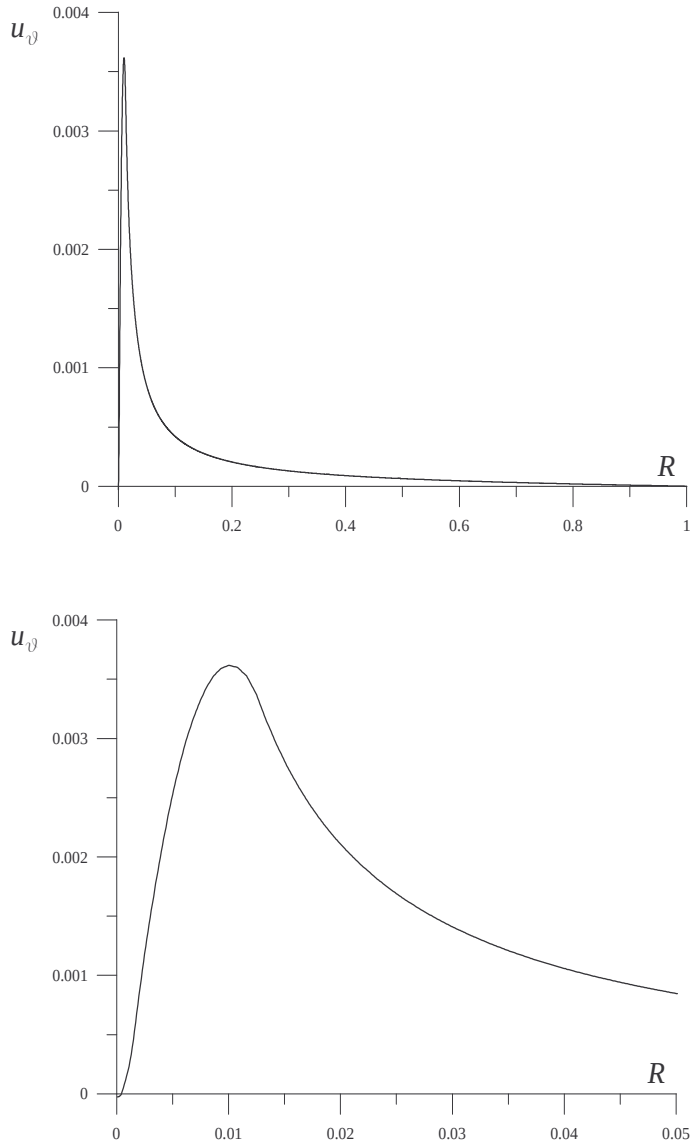

Figure 9: Displacement field $u_\vartheta(R)$ for the *asymmetric* constraint solution. Two scales of R.

The angle of rotation of the central core is more easily appreciated by examining the field $\vartheta(R) - \Theta$, defined again as in Figure 1. We show this in Figure 10 for two scales of R. It is clear that the angle of rotation of a core of small radius is nominally π.

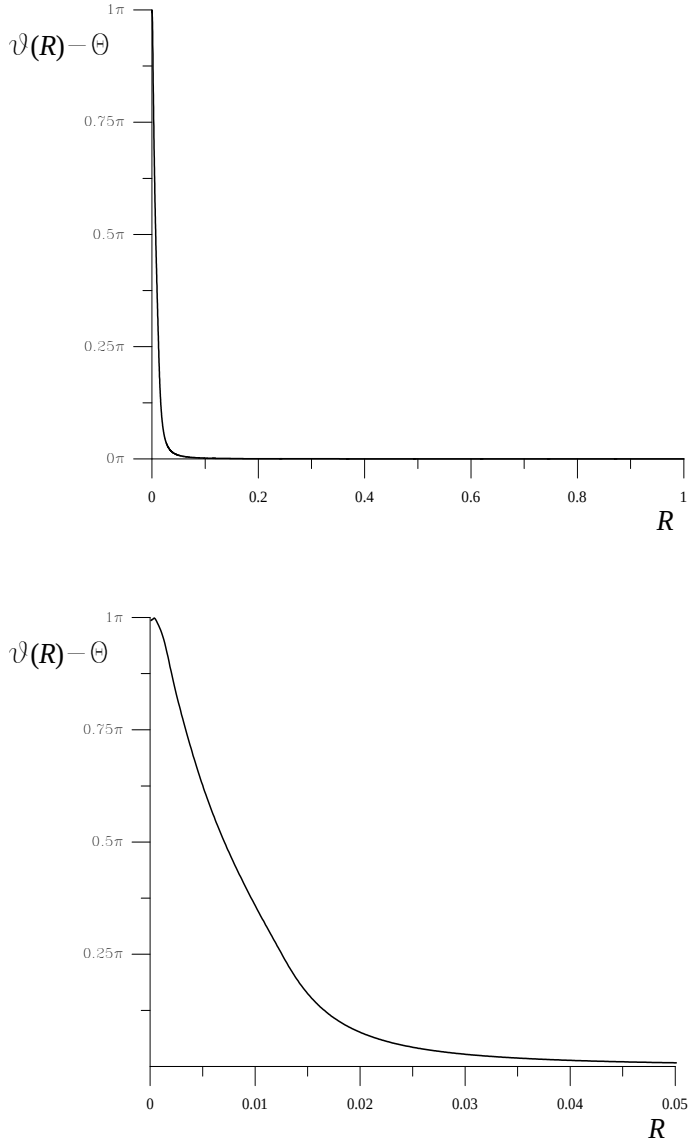

Figure 10: Field $\vartheta(R) - \Theta$ for the asymmetric constrained solution. Two scales of R.

The corresponding deformation is associated with a positive determinant of the deformation gradient field, even though the infinitesimal strain components e_{rr} and $e_{\theta\theta}$ both become strongly negative in the vicinity of the origin. This limiting behavior is demonstrated in Figures 11 and 12, where e_{rr} and $e_{\theta\theta}$ are plotted as a function of R. Indeed, for an exactly rigid rotation there is a non-zero infinitesimal strain and when $e_{rr} = e_{\theta\theta} < 0$ the rotation angle is 180°. In fact, in two dimensions a polar inversion is equivalent to a rotation of 180° about an axis perpendicular to the plane through the pole. This 180° rotation of a core is how the classical Lehknitskii solution is altered within the confines of the injectivity constraint and with minimal energy consumption. Of course, here a shear modulus is sufficiently small to accomodate energetically a large azimuthal shear which makes the 180° core rotation possible.

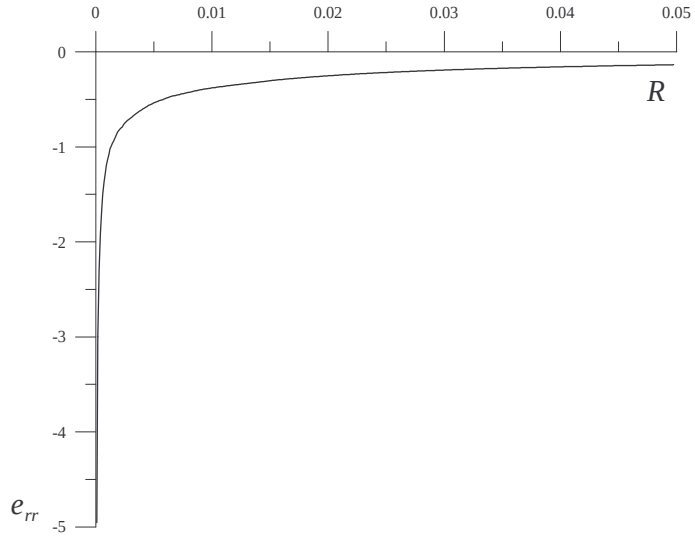

Figure 11: Asymmetric solution: Infinitesimal radial strain e_{rr}.

The infinitesimal shear strain $\gamma_{r\theta}$ is shown in Figure 13. Note that $\gamma_{r\theta}$ is practically zero sufficiently far from the center where the solution tends to become radially symmetric and of the classical Lehknitskii type. Notice, also, that in a neighborhood of the center of the disk, both positive and negative infinitesimal shearing strains are attained; we believe that this is due to the effect of large rotation. The components of the constitutive stress σ_{rr}, $\sigma_{\theta\theta}$ and $\sigma_{r\theta}$, defined as in (2.1), are plotted as a function of R in Figures 14, 15 and 16, respectively.

The field λ_δ of (3.5), representing an approximation of the Lagrange multiplier field λ^* of (2.20), is shown in Figure 17. As reported earlier, we know that $\lambda_\delta \to \lambda^*$ for $\delta \to +\infty$ and, in the case of Figure 17, the parameter $\delta = 10^9$ is quite large. Numerical experiments have confirmed that the form of λ_δ does not change if δ is further increased. The graph of the Lagrange multiplier field as a function of the distance R from the disk center is shown in Figure 18. Note, here, that the Lagrange multiplier takes large but finite values and, as already mentioned, it vanishes outside of a certain radius as well as in a neighborhood of the center of the disk because the injectivity constraint is not active in these two regions.

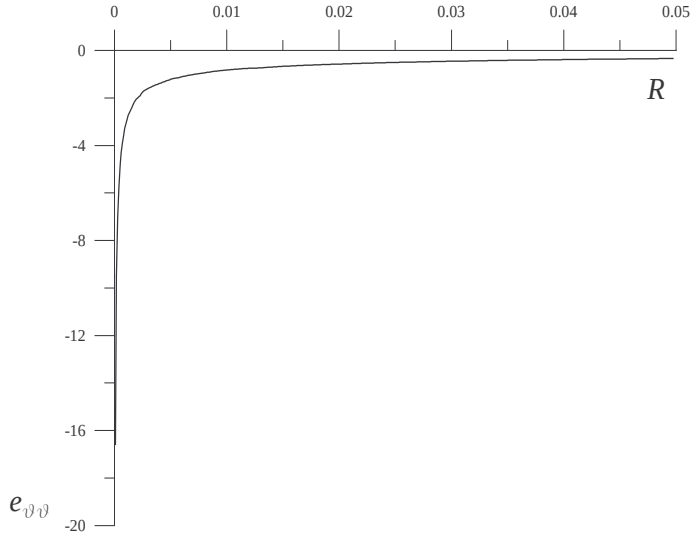

Figure 12: Asymmetric solution: Infinitesimal hoop strain $e_{\theta\theta}$.

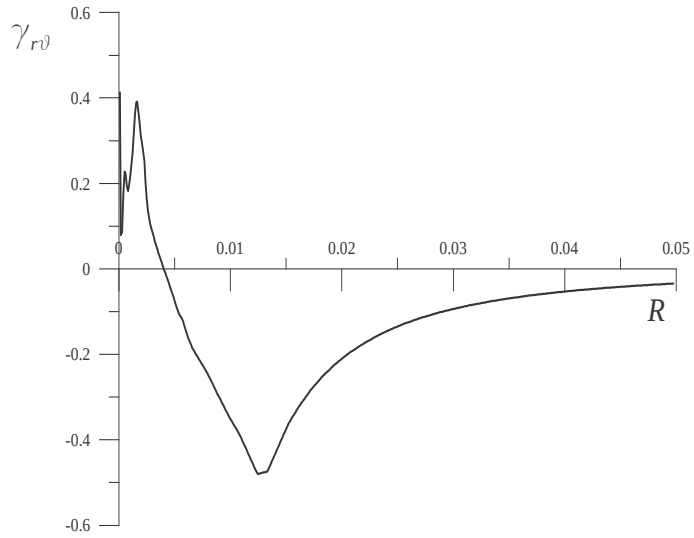

Figure 13: Asymmetric solution: Infinitesimal shear strain $\gamma_{r\theta}$.

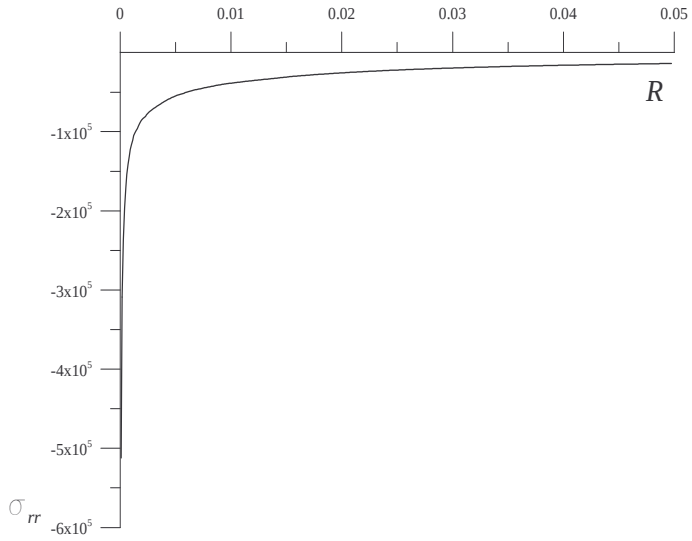

Figure 14: Asymmetric solution: Constitutive radial stress component σ_{rr}.

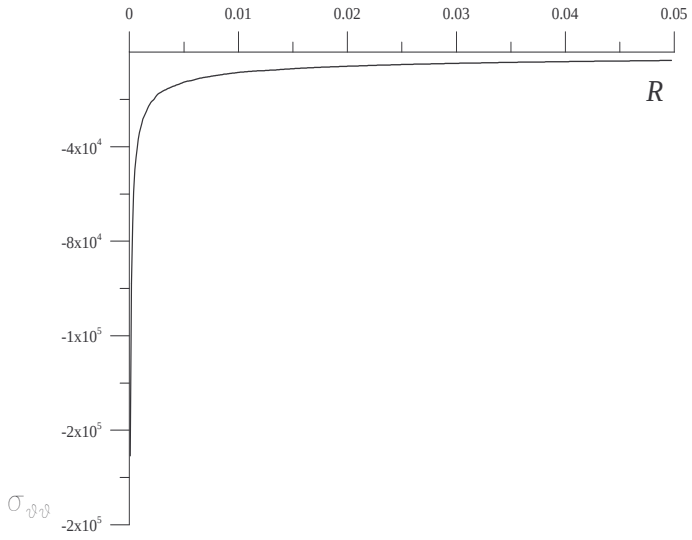

Figure 15: Asymmetric solution: Constitutive hoop stress component $\sigma_{\theta\theta}$.

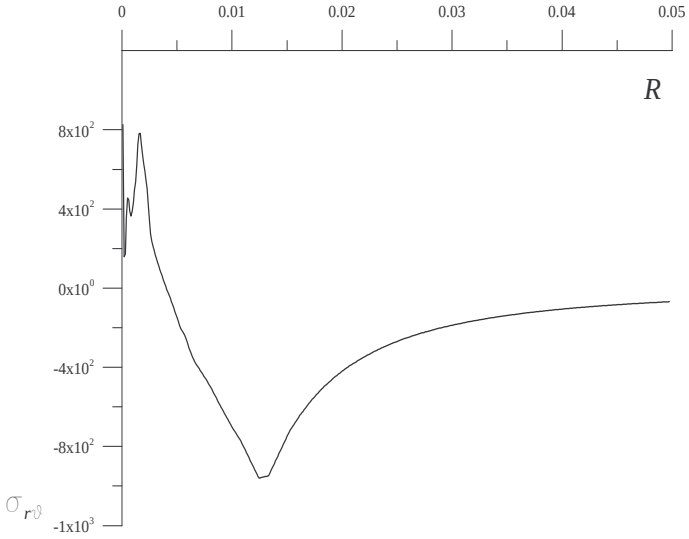

Figure 16: Asymmetric solution: Constitutive shear stress component $\sigma_{r\theta}$.

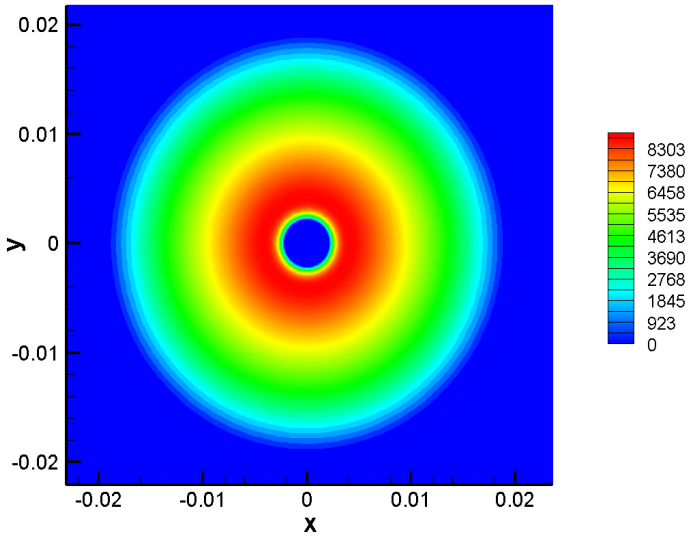

Figure 17: Numerical approximation λ_δ of the Lagrange multiplier field for the asymmetric constrained solution. Here, $\delta = 10^9$.

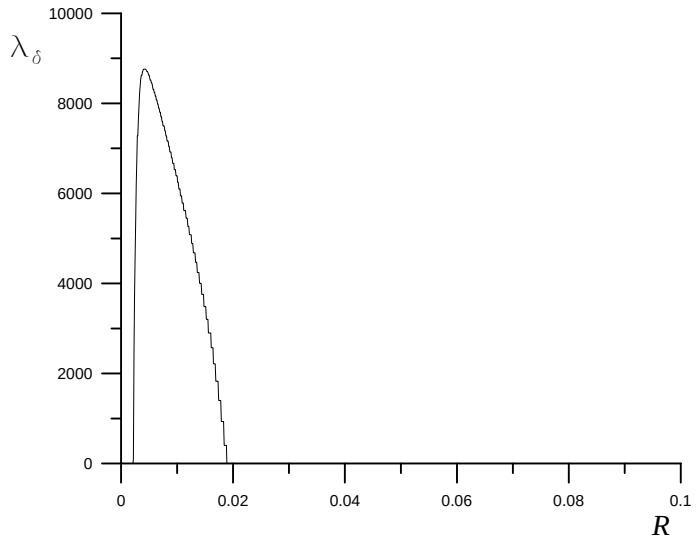

Figure 18: The Lagrange multiplier λ_δ as a function of R for $\delta = 10^9$.

The elastic parameter that influences the transition between the symmetric and asymmetric solutions is the shear modulus c_{66}. In Figure 19 we show the field $u_\vartheta(R)$ for different values of the elastic parameter c_{66}; here, we fix the remaining material moduli at the values reported in Tables 1 and 2. It is clear from the graph that $u_\vartheta \to 0$ as c_{66} increases, i.e., the stiffer the shear modulus, the more the solution becomes radially symmetric. This is not surprising, since an increase in the shear stiffness diminishes the tendency for any possible core rotation. We conclude that a bifurcation instability occurs when the shear stiffness is sufficiently small–a defect-like instability.

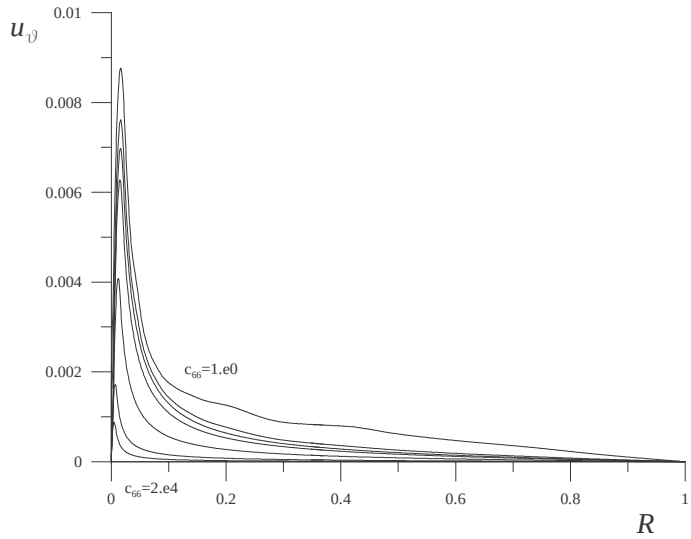

Figure 19: The field $u_\vartheta(R)$ for different values of the elastic modulus c_{66}.

Our numerical experiments have shown that the threshold value of c_{66} that marks the transition from the symmetric to the asymmetric solution is approximately $2.0e4$. As c_{66} becomes sufficiently small (and the value $c_{66} = 1$ in Figure 19 qualifies), a vanishing resistance is offered against the relative rotation of concentric disk portions. The wiggly appearance of the corresponding graph in Figure 19 is a symptom of a numerical ill-conditioning that is naturally associated with this kind of material instability.

4.3 Numerical remarks

The proposed numerical strategy to solve the constrained minimization problem consists of outer and inner loop computations. The outer loop sets a starting point and an approximating objective function through a proper choice of the parameter δ in (3.6); the possible strategies for such a choice will be explained. The corresponding optimization problem is solved in the inner loop using Newton's method coupled with a line-search procedure, as discussed in Section 3. The crucial points in this procedure are the following:

1. INITIAL GUESS:

The interior penalty method requires the specification of a starting point $\mathbf{u}_0$ which respects the boundary condition and does not violate the local injectivity constraint. If the problem at hand was a mixed boundary value problem with homogeneous Dirichlet

boundary conditions, the natural choice is the undistorted reference configuration, as was chosen in [1]. When the displacement is assigned on the boundary, as in the present case, a few difficulties may be encountered because, in general, it is not evident how to specify a field that, while respecting the Dirichlet boundary condition, does not violate the constraint. In the computations of this work, our starting point, $\mathbf{u}_0$, is chosen to be the equilibrium displacement field for a homogeneous, isotropic disk, which is obtained by assuming $c_{11} = c_{22}$ in (2.7) (linear radial displacement).

2. OPTIMIZATION OF THE NUMERICAL SCHEME:

Once the inner iteration loop has been completed, so that the corresponding optimization problem associated with an assumed value of δ has been solved, the outer loop proceeds by increasing the value of δ by a multiplicative factor $\mu > 1$ and redoing the inner loop.

Choice of μ: The choice of μ involves a "trade-off decision" in the number of inner and outer iterations that are required. If μ is small (for example, nearly 1), then at each outer iteration δ is increased by a small factor. Consequently, the iterate $\mathbf{u}$ obtained at the end of the previous inner loop, is a very good initial point for the Newton process that is to be carried out for the next inner iterative loop. Thus, the number of Newton steps necessary to solve the corresponding optimization problem is relatively small. On the other hand, the number of outer iterations consequently is large. Our numerical experiments have shown that when μ is between 3 and 100, one effect offsets the other, so that the total number of Newton steps remains approximately constant. This means that the choice of μ is not particularly critical, and in this work we have chosen $\mu = 10$.

Choice of δ: The initial choice for the parameter δ may produce a dramatic effect on the running time of the algorithm. A parameter that is too small may cause the relevant system of equations to be ill-conditioned. Here, the trade-off is simple: If δ is chosen too large, the first inner iteration loop will require too many iterations. On the other hand, if δ is chosen too small, the algorithm will require additional outer iterations.

In Figures 20-22 we show the numerical solutions for $r(R) - R$ and $u_\vartheta(R)$ that are obtained by increasing the penalty parameter δ. Each graph corresponds to the solution of the optimization problem defined in (3.3) corresponding to a specific value of δ. Note that small values of the parameter δ (starting from $\delta = 10^{-3}$) have been considered. It should be observed that no spurious field is obtained even for the smallest δ, and the convergence of the outer iteration loop is quite accurate. This finding is somewhat different from what was reported in [1]. There, the solution associated with the smallest values of δ was quite inaccurate.

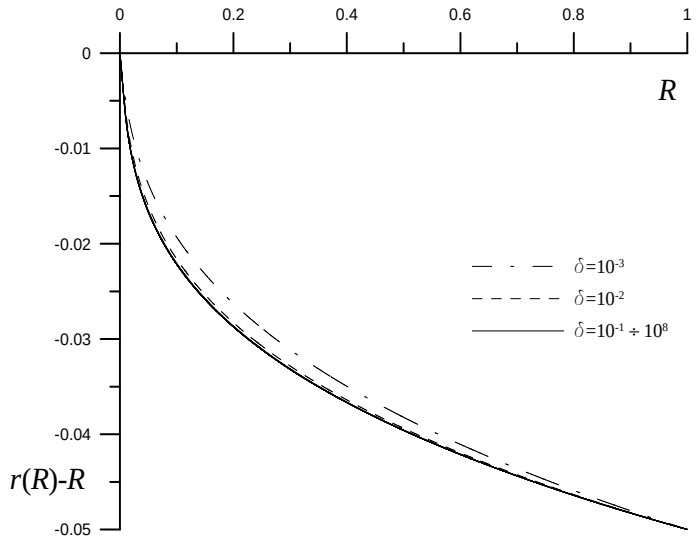

Figure 20: The field $r(R) - R$ for the symmetric constrained solution for different values of the penalty parameter δ.

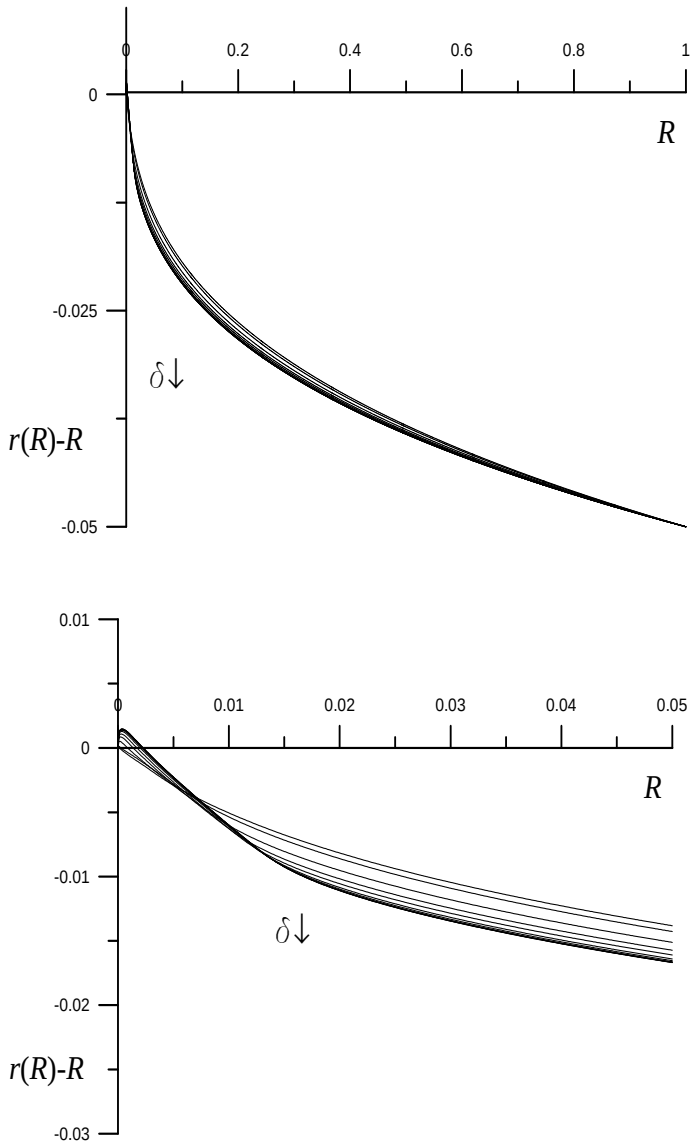

Figure 21: The field $r(R) - R$ for the asymmetric constrained solution for different values of the penalty parameter δ; two scales of R.

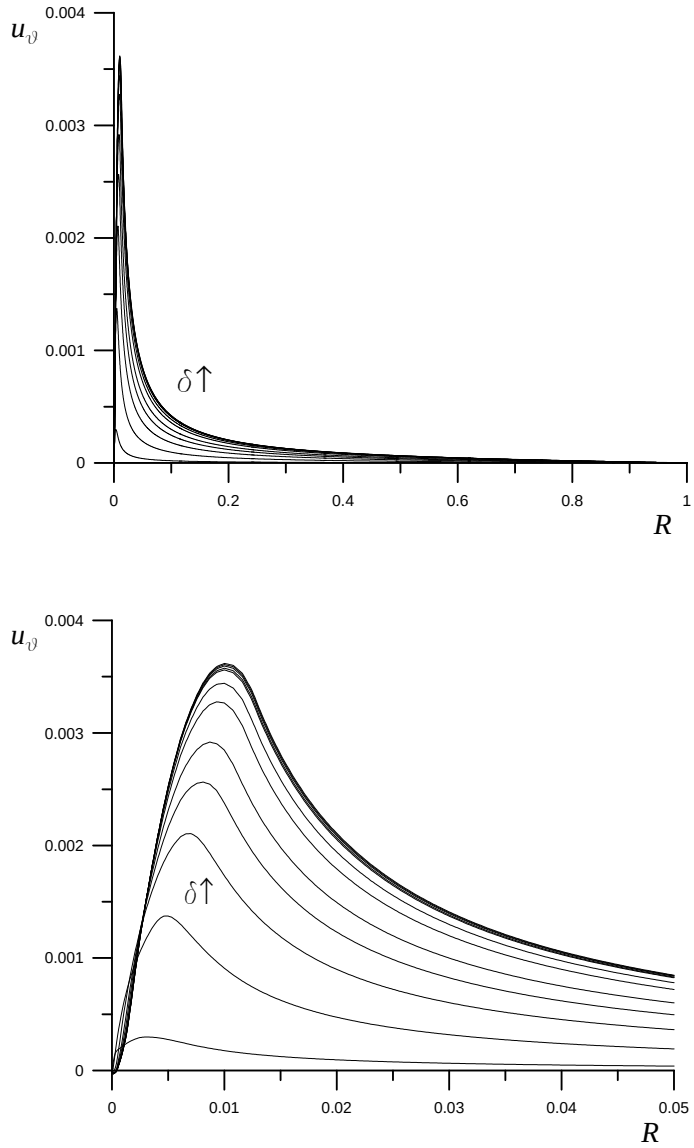

Figure 22: The field $u_\vartheta(R)$ for the asymmetric constrained solution for different values of the penalty parameter δ; two scales of R.

Truncated Newton methods were introduced in the early 1980's [11] and have gained wide popularity. Such methods rely upon the idea that an exact solution at every step of the iteration is unnecessary and, indeed, can be computationally wasteful in the framework of a basic descent method. Even a rough approximation of the descent direction can suffice when the objective function is not well approximated by a convex quadratic function and, when a solution of the minimization problem is approached, more effort in solving the the resulting system of algebraic equations using the Newton-Raphson method may be warranted.

3. ILL-CONDITIONING:

When the parameter δ is large, the functional (3.6) is difficult to minimize by Newton's method because its Hessian varies rapidly near the boundary of the admissible set. This problem can be overcome by an iterative method: Solve the minimization problem for some initial δ, and then increase δ (and therefore the accuracy of the approximation) at each step, starting each Newton minimization at the solution of the problem corresponding to the previous value of δ.

5 Discussion and conclusions

The constrained theory here applied represents an attempt to remove the physical unacceptability of material interpenetration that occurs in many classical problems, usually involving stress singularities. The theory, first proposed in [7], attempts to maintain the original framework of linear elasticity theory, but adds an internal requirement, i.e., the constraint of local injectivity, that aims at modelling, in the simplest way, the strong repelling forces that occur between the material particles when the separation distance between them tends to become zero. This constraint represents, in a certain sense, a "minimal" requirement to be added to the linear elasticity theory, without having to resort to the whole complexity of a full non-linear elasticity theory. In fact, linear elasticity theory gives very accurate results at points sufficiently far from singular points, and must be rejected only in very small regions of singular behavior. Moreover, this approach preserves the definition of material symmetries, which have a more complicated characterization in non-linear theories.

The elementary classical Lekhnitskii problem for an aelotropic disk, proposed as the paradigmatic example of the constrained theory, has been revisited. The main novelty of this work is that the problem has been solved numerically without enforcing an assumption of radial symmetry, which reduces the problem to one of one-dimension. Of course, the solution of the full 2-D problem presents considerable more difficulty from a numerical point of view than does the 1-D problem. An *ad hoc* numerical strategy has been adopted which solves a sequence of specially constructed unconstrained optimization problems within the framework of the internal penalty formulation.

Our approach and numerical experiments have allowed us to discover and to discuss asymmetric minimizers to a problem that was thought to possess only radially symmetric solutions, highlighting the occurrence of internal material bifurcation instabilities. This phenomenon essentially is due to the non-linear character of the constraint. For the disk problem, the 180° rotation of the central core gives rise to an asymmetric minimizing deformation field and this deformation is possible because the shear modulus, which governs the azimuthal shear, is sufficiently small.

In general, the proposed constrained theory of [7] may be particularly relevant to model the response of brittle materials, such as glass, whose behavior is practically linear elastic

up to rupture, without the mitigating effect of plasticity or damage. Possible applications may be envisaged in a number of classical problems, such as the bonded punch problem, already discussed in [2], or in linear elastic fracture mechanics.

References

[1] Aguiar, A.R., Local and global injective solutions of the rotationally symmetric sphere problem, *Journal of Elasticity*, **84**, pp. 99-129, 2006.

[2] Aguiar, A.R., Fosdick, R., Self intersection in elasticity, *Int. J. Solids and Structures*, **38**, pp. 4797-4823, 2001.

[3] Ball, J., Convexity condition and existence theory in non-linear elasticity, *Arch. Ration. Mech. Analysis*, **63**, pp. 337-403, 1977.

[4] W. Bangerth, R. Hartmann, G. Kanschat, *deal.II Differential Equations Analysis Library, Technical Reference* (2005). http://www.dealii.org/.

[5] De Giorgi E., Un esempio di estremali discontinue per un problema variazionale di tipi ellittico, *Boll. Unione Matematica Italiana*, **1**, pp. 135-137, 1968.

[6] Fosdick, R., Obeidat, K., Royer-Carfagni, G., Stolarski, H., Numerical analysis of elastic problems with injectivity constraint, *ECCM-2001 2nd European Conference on Computational Mechanics*, p. 1082 (abstract), pp. 1-15 (*in extenso* on CD-ROM), Krakow, 2001.

[7] Fosdick, R., Royer-Carfagni, G., The Constraint of Local Injectivity in Linear Elasticity Theory, *Proceedings of the Royal Society of London*, **A457**, pp. 2167-2187, 2001.

[8] Lekhnitskii, S.G., *Anisotropic Plates*, Gordon & Breach, New York, 1968.

[9] Luenberger, D.G., *Linear and Nonlinear Programming*, 2nd ed., Addison-Wesley, Reading, 1984.

[10] Nash, J., Continuity of solutions of parabolic and elliptic equations, *Am. J. Mat.*, **80**, 1958.

[11] Nash, S.G., A survey of truncated-Newton methods, *J. Comp. Appl. Math*, **124**, 2000.

[12] Nocedal, J., Wright, S.J., *Numerical optimization*, Springer Verlag, New York, NY, 1999.

[13] Podio-Guidugli, P., De Giorgi's counterexample in elasticity, *Quart. Appl. Math.*, **34**, pp.411-419, 1977.

[14] Simo, J.C., Taylor, R.L., Penalty function formulations for incompressible nonlinear elastostatics, *Comp. Meth. Appl. Mech.*, **35**, pp. 107-118, 1982.

[15] Tarn, J.Q., Stress singularity in an elastic cylinder of cylindrically anisotropic material, *Journal of Elasticity*, **69**, pp. 1-13, 2006.

[16] Wright, M.H., Interior methods for constrained optimization, *Acta Numerica 1992*, pp. 341-407, Cambridge University Press, New York, USA, 1992.